

Robustness of Size Selection and Spectroscopic Size, Thickness and Monolayer Metrics of Liquid-Exfoliated WS₂

Lucas Ueberricke, Jonathan N. Coleman, and Claudia Backes*


Liquid exfoliation and centrifugation based size selection has emerged as widely applied technique to produce nanosheets in a solution-processable form. Quantitative spectroscopic metrics to extract nanosheet size, thickness and monolayer content from optical spectra have previously been established. Such metrics are extremely useful and can be used to optimise the production technique (for example on scale-up) and size selection. However, it is not clear whether exfoliation, size selection, and spectroscopic metrics are robust or whether the result depends on the starting material or subtle details of the processing and analysis. By comparing two batches of WS₂ exfoliated and size-selected in aqueous surfactant solution using different starting materials, protocols and equipment in each step, we show that the nanosheet size obtained after different steps in a cascade centrifugation is highly reproducible. A detailed statistical analysis on the nanosheet dimensions revealed well-defined relationships between nanosheet mean thickness and monolayer content. Spectroscopic metrics for nanosheet layer number, lateral size (from extinction) and monolayer content (from Raman/photo-luminescence) do not depend on sample type and measurement conditions, albeit the data analysis may require adjustment as discussed.

1. Introduction

During the past few years, 2D materials have been widely explored and identified as diverse materials with fascinating properties and application potential in areas from optoelectronics to energy.^[1–9] Very recently, additional excitement was kindled about exploiting the properties of 2D materials in printed devices.^[10–12] This requires 2D materials of various kind in dispersion that can be used to form a printable ink.^[13]

L. Ueberricke, Dr. C. Backes
Chair of Applied Physical Chemistry
Ruprecht-Karls University Heidelberg,
Im Neuenheimer Feld 253, 69120 Heidelberg, Germany
E-mail: backes@uni-heidelberg.de

Prof. J. N. Coleman
School of Physics and CRANN & AMBER Research Centres
Trinity College Dublin,
Dublin 2, Ireland

 The ORCID identification number(s) for the author(s) of this article can be found under <https://doi.org/10.1002/pssb.201700443>.

DOI: 10.1002/pssb.201700443

Regardless of the targeted application, the performance in the device will to some extent always depend on the quality of the dispersion at the beginning of the process chain and critically, the nanosheet size and thickness. Liquid phase exfoliation (LPE) is considered as rather simple, readily accessible and potentially scalable method capable of producing dispersions containing various 2D nanosheets.^[13–19] In LPE, a starting material (crystal or powder) is immersed into an appropriate solvent (such as N-methylpyrrolidone)^[20] or aqueous surfactant solution^[21] and subjected to sonication or shear.^[13–19] The energy input overcomes the weak interlayer interaction between the layers and the solvent or surfactant prevents the nanosheets from restacking in the liquid. As a result, colloidal stable dispersions are obtained that can be further processed.

Despite its potential, LPE suffers from the disadvantage that broad size and thickness distribution in the stock dispersion are obtained. Since the size (both layer number and lateral dimension) determines the properties of the nanosheets, it is

extremely important to control this. Typically, size selection techniques by controlled centrifugation are applied to narrow down size and thickness distributions.^[13,22,23] Among the numerous centrifugation strategies, liquid cascade centrifugation^[24] has proven extremely useful, as it gives access to a number of size and thickness distributions from the same stock dispersion with little wastage of material making it ideal to study size-dependent properties. In addition, it can be applied to a broad range of materials in both solvent and surfactant solutions.^[25–31]

However, in general, precise control over size and thickness and reproducibility are still an issue- both in terms of the initial exfoliation as well as the size selection. This is mostly because it is extremely time consuming to measure size and thickness distributions by statistical microscopy making process optimisation very tedious. To this end, we have previously developed quantitative size and thickness metrics for LPE MoS₂^[32] and WS₂^[24] based on optical extinction spectroscopy. We have realised that the extinction spectra do not only change with thickness of the material (reflected in the position of the

A-exciton), but also with lateral dimensions of the TMD nanosheets (reflected in different peak intensity ratios). By quantifying lateral dimensions and thicknesses by statistical microscopy, we were able to establish metrics that allow us to extract the layer number and lateral dimensions from extinction spectra. We have developed further metrics based on the measurement of the Raman and photoluminescence in liquids to determine the monolayer content in WS₂ dispersions quantitatively.^[24]

In this report, we assess whether the liquid exfoliation, size selection by liquid cascade centrifugation and size analysis by microscopy and optical spectroscopy is reproducible. This is achieved by comparing the result of two batches of size-selected WS₂ dispersions using a similar protocol, but with slight variations. In particular, each step of the production and characterisation was performed using different equipment. In general, we find the procedure to be extremely robust. Based on the results, an improved data analysis is suggested and refined metrics equations presented.

2. Results and Discussion

To test the robustness of the size selection and in particular spectroscopic metrics, two batches of WS₂ were prepared, size-selected, and characterised microscopically and spectroscopically using comparable protocols, but different equipment in each step. For details see the methods section and Table 1. In brief, WS₂ powder was exfoliated by tip sonication in aqueous sodium cholate (SC, 2 g L⁻¹, 80 mL). This stock dispersion contains a very broad size and thickness distribution of nanosheets and was subjected to controlled centrifugation to extract a range of fractions with narrower size distributions. This was achieved by liquid cascade centrifugation (LCC) which is described in detail elsewhere.^[24] This technique is an iterative centrifugation, where the stock dispersion is first centrifuged at low centrifugal acceleration (expressed as relative centrifugal field, *RCF*, in units of the earth's gravitational field, *g*) and the sediment containing unexfoliated material discarded. The supernatant is subjected to another centrifugation at slightly higher *RCF*. Again supernatant and sediment are separated and the sediment containing large/thick nanosheets collected in fresh H₂O-SC, while the supernatant is again centrifuged at higher *RCF*. This is continued for multiple steps. In this case, 6–7 fractions per batch were produced in this way, but with different centrifugal accelerations and using different centrifuges and thus vial geometries in the two batches. As sample nomenclature, we therefore find it feasible to indicate both the lower and upper centrifugation boundary of the fraction. For example, if the supernatant after centrifugation with *RCF* = 5000 × *g*-force (5 kg) is centrifuged at 10 000 *g* and the sediment collected after this step, we refer to the sample as 5–10 kg.

To assess the result of the size selection, the various fractions were deposited on Si/SiO₂ wafers and subjected to statistical atomic force microscopy. For each sample, 150–400 individual nanosheets were examined and their length (defined as longest dimension), width (dimension perpendicular to the length) and thickness measured. The apparent AFM thickness is typically overestimated compared to the theoretical thickness of the

Table 1. Summary of the variations in parameters and their impact on the size selection or spectroscopic metrics.

Parameter variation	Impact	Sort of impact and identified threshold
Sonication		
Nominal power of sonicator (500 vs. 750 W)	No	
Amplitude in sonication	Yes	Degree of exfoliation lower for amplitudes <50%
Centrifugation		
Vial geometry	Yes	Depending on rotor/vial geometry, the filling height in the vial has a non-negligible effect on obtained size in particular above 8.5 cm (for 2 h centrifugation)
RCF boundaries	No	(if filling height consistent)
Characterisation		
AFM model	No	
AFM cantilever and scan resolution	Yes	Different correction for lateral sizes, but error <10%
Extinction/absorbance spectrometer model	No	
Extinction measurement conditions	Yes	Increments of 1 nm more suitable to extract $\langle N \rangle$ increments 0.5 nm more suitable to determine ML V_f ; can be overcome by appropriate smoothing
Raman model and acquisition mode	No	
Raman excitation wavelength	No	(only tested for 532 and 473 nm)
Focus of Raman laser	Yes	Focus has to be above droplet surface ^[54]
Laser power	Yes	Heating and degradation at higher powers (dependent on sample, $\langle L \rangle$, $\langle N \rangle$, concentration; needs to be tested in each case)

nanosheet with a given layer number, especially in the case of liquid-exfoliated samples. To convert the AFM thickness to layer number, the apparent height of one layer must be known. In the case of MoS₂ and WS₂, this was previously found as 1.9 nm.^[24,32] From the AFM statistics, layer number ($\langle N \rangle$) and length histograms ($\langle L \rangle$) are obtained (Supporting Information, Figures S1–S4) and arithmetic mean values of the nanosheet dimensions extracted ($\langle N \rangle$, $\langle L \rangle$). AFM suffers from the disadvantage that the nanosheet length is also overestimated due to broadening from the cantilever and pixilation effects. This can be corrected for by analysing a set of samples with varying length by both statistical AFM and transmission electron microscopy (TEM) which is more accurate in determining the lateral dimensions, but often fails to give reliable values for nanosheet layer number. By plotting $\langle L \rangle$ from AFM and TEM versus each other, an equation can be extracted to account for the AFM broadening (Figure S5) to yield corrected values for the mean nanosheet length, $\langle L \rangle_{\text{cor}}$. Note that this correction factor is dependent on the measurement conditions, microscope specifications and cantilevers used.

In **Figure 1A** and **B**, the as determined arithmetic mean of corrected nanosheet length and layer number are plotted as function of the midpoint of *RCF* in the centrifugation cascade for the two sample batches. As previously shown for LCC,^[24] $\langle L \rangle_{\text{cor}}$ decreases as $(g\text{-force})^{-0.5}$, while $\langle N \rangle$ falls off as $(g\text{-force})^{-0.4}$.

Importantly, data from both batches collapse on the same curve confirming that both size selection and size determination are robust. Note that we find this to be the case, as long as the exfoliation and size selection protocols are kept similar (details see SI section 3).

Another way to analyse the AFM data is to estimate the volume of each nanosheet (as length multiplied by width and thickness) in each sample and thus to determine volume fractions, V_f for nanosheets of a given layer number N . This allows to weight the mean layer number by the volume to obtain the V_f -weighted mean $\langle N \rangle_{V_f\text{-weighted}}$, rather than the arithmetic mean via Eq. (1):

$$\langle N \rangle_{V_f\text{-weighted}} = \frac{\sum_{\text{all}} N^2 L W}{\sum_{\text{all}} N L W} \quad (1)$$

While this appears to be a more accurate description for the layer number when a correlation with spectroscopic data is targeted, either arithmetic or V_f -weighted mean can be used for a correlation because they are related as $\langle N \rangle_{V_f\text{-weighted}} = 0.4 + 0.6 \langle N \rangle$ (see Figure S8). To test the validity of our statistics, we plot the V_f as a function of nanosheets with a given thickness N in **Figure 2C,D**. Data for three sizes of both batches are shown. In all cases, the data can be fit to a log-normal distribution (similar to the log-normal distributions of the N and L histograms). From this fit, the median layer number, x_c , can be extracted which is identical to the V_f -weighted mean $\langle N \rangle$ as shown in **Figure 1E**. Note that this is only the case when the statistics are robust and a large enough number of nanosheets have been counted. From these fits, the V_f of monolayers (ML V_f) in the dispersion can be extracted at high accuracy even for low monolayer contents. The ML V_f is plotted as function of $\langle N \rangle_{V_f\text{-weighted}}$ in **Figure 1F**. A well-defined exponential relation is observed as would be expected. This means that the ML V_f can be calculated from the mean thickness according to Eq. (2):

$$\text{ML } V_f = 2.15 \times 10^{(-0.78 \cdot \langle N \rangle_{V_f\text{-weighted}})} \quad (2)$$

Figure 1. Result of the AFM statistical analysis of WS₂ liquid-exfoliated in SC and size-selected by liquid cascade centrifugation. Two different batches are compared. A) Mean nanosheet length (corrected for cantilever broadening, $\langle L \rangle_{\text{cor}}$) as function of *RCF*. B) Mean nanosheet layer number (arithmetic mean, $\langle N \rangle$) as function of *RCF*. C–D) Volume fraction, V_f as function of layer number for three size-selected samples LCC. Centrifugal accelerations are indicated in the panel legends. The data is fit to a log-normal function. From such fits, the median of the distribution, x_c , can be extracted. Due to variations in the centrifugation cascade, the samples of batch 1 and 2 are slightly different and the data of panel C (batch 1) and D (batch 2) is not directly comparable. E) Plot of x_c from the log-normal fit of V_f as function of N versus the mean layer number weighted by volume (where volume is estimated by nanosheet length \times width \times thickness). Values are identical for the respective fractions as indicated by the grey line of $y=x$ indicating robust statistical analysis. F) Plot of the monolayer volume fraction (ML V_f) as function of volume-weighted $\langle N \rangle$ (main plot log-log). An additional data point at a ML V_f of 1 which would lead to a $\langle N \rangle$ of 1 is added to improve the accuracy of the fit (cyan data point). The inset shows the plot on a linear scale. A robust correlation that can be fit well to an exponential decay (dashed blue line) is seen across both batches that allows to extract the ML V_f from $\langle N \rangle$.

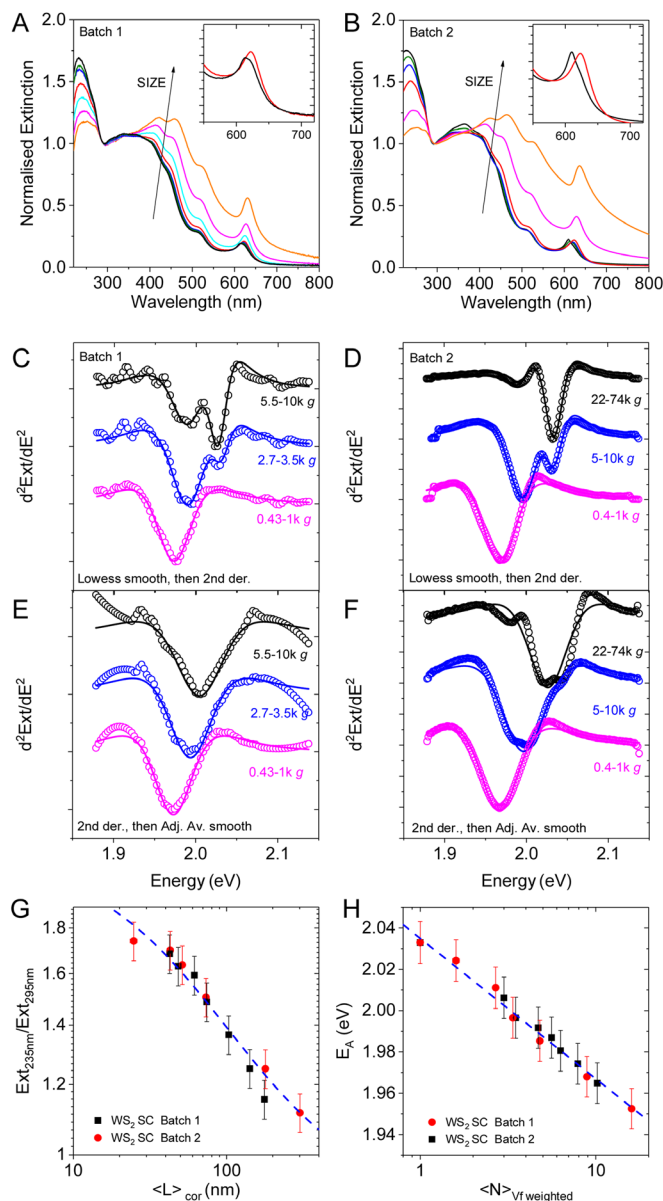


Figure 2. Extinction spectroscopy and derived length and thickness metrics for two batches of liquid-exfoliated WS₂. A-B) Optical extinction spectra normalised to the local minimum at 294 nm of WS₂ dispersions containing different size/thickness distributions. Inset: A-exciton region for a subset of samples. A) Batch 1, B) Batch 2. C-F) Second derivative spectra of the A-exciton region for a subset of samples. C-D) Second derivative obtained after smoothing the spectrum with Lowess (12 points per window) and then differentiating twice. This data processing is ideal to resolve the splitting of the monolayer component (≈ 2.033 eV) and few-layer component. The data is fit well to the sum of the second derivative of two Lorentzians. C) Batch 1, D) Batch 2. E-F) Same data processed differently to force the peaks to merge achieved by first differentiating twice and then smoothing the derivative with Adjacent Averaging (30 points per window). The data is fit to one Lorentzian to extract the mean exciton energy. E) Batch 1, F) Batch 2. G) Extinction intensity ratio as function of $\log(L)$. The blue dashed line is a fit according to the model assuming different extinction coefficients at edge and centre, respectively.^[32] This ratio gives a robust metric for mean nanosheet length according to Eq. (3) with data for both batches collapsing on a mastercurve. H) A-exciton energy as function of the volume-fraction weighted layer number. The blue dashed line is an exponential fit resulting in a robust metric for mean nanosheet thickness according to Eq. (4).

subjected to extinction spectroscopy and Raman/photoluminescence measurements. Normalised extinction spectra of the different fraction after LCC are shown in Figure 2A, B. The typical changes in spectral shape with nanosheet size/thickness are observed in both cases. These can be summarised as follows:

firstly, edges of nanosheets are electronically different from the basal planes and therefore show different absorbance coefficients at a given wavelength. Hence, the lateral sheet size can be extracted from peak intensity ratios. Secondly, the nanosheet thickness is reflected in shifts of the excitonic transitions. This is

related to changes in the band structure as well as thickness dependent dielectric screening of the excitons.^[24,32,34–36] This shift is clearest for the A-exciton centered at 610–620 nm in WS₂ (inset in Figure 2A,B). In both MoS₂ and WS₂, we previously found that the A-exciton energy scales exponentially with the layer number.

Due to the scattering background^[32,33,37] in the larger/thicker nanosheet dispersions which leads to artificial peak shifts, the A-exciton energy is best determined from the second derivative spectra. Examples are shown in Figure 2C–F for both batches. Typically, smoothing is required to reduce the noise in the second derivative. However, care must be taken, as the resultant plot will be dependent on the smoothing method and the number of data points used in each local regression (points of window).^[24] For example, if the spectrum is smoothed with the Lowess method and then differentiated twice, the A-exciton can split into two components (Figure 2B,C). At higher energy (≈ 2.023 eV), the monolayer can be discerned as well separated species from the sum of all few-layers at lower energy. This is useful, as it can be used to extract the monolayer content in the sample by fitting the spectra to the sum of the second derivative of two Lorentzians (solid lines in Figure 2B,C).^[24] In this case, increasing the number of data points in the spectrum will improve the reliability of the fit. For example, the spectra in batch 1 (Figure 2B) which were measured in 1 nm increments still show a background noise, while this significantly improved for batch 2 (Figure 2C, 0.5 nm increments).

However, resolving this splitting between monolayer and few-layer A-exciton energies may not always be desired, as it makes it difficult to assess the mean peak position which can be related to $\langle N \rangle$ or $\langle N \rangle_{\text{VF-weighted}}$. In this case, it is required to force the peaks to merge as much as possible. This can be achieved by first differentiating twice and then smoothing with the Adjacent Averaging method using more data points in each local regression. Examples are shown in Figure 2E,F. In the spectra that were measured with 1 nm increments (Figure 2E), this works very well and the data can be fit with the second derivative of only one Lorentzian (solid lines) even in the samples with a relatively high monolayer content (5.5–10 kg). This becomes more difficult in the spectra that were measured with 0.5 nm increments (Figure 2F). Nonetheless, a fit can be forced through the data to extract the mean A-exciton peak position.

After this assessment of the data analysis, we now compare the result from the two batches in the length and thickness metric plots, respectively. As we have previously shown, the extinction intensity ratio $\text{Ext}_{235\text{nm}}/\text{Ext}_{290\text{nm}}$ is a suitable measure for the lateral size of the WS₂ nanosheets.^[24] This is confirmed by the plot of $\text{Ext}_{235\text{nm}}/\text{Ext}_{290\text{nm}}$ as function of $\langle L \rangle$ in Figure 2G which shows that the data from both batches fall on the same curve. Note that we have added data points ranging to both smaller and larger nanosheets in batch 2 which gives a refined fit equation to relate the extinction intensity ratio $\text{Ext}_{235\text{nm}}/\text{Ext}_{290\text{nm}}$ to the mean nanosheet length $\langle L \rangle$ by Eq. (3):

$$\langle L \rangle = \frac{140.5 - 65\text{Ext}_{235}/\text{Ext}_{290}}{\text{Ext}_{235}/\text{Ext}_{290} - 0.89} \quad (3)$$

Similarly, the data from both batches collapses on the same curve for the plot of the A-exciton energy as function of mean layer number $\langle N \rangle_{\text{VF-weighted}}$ in Figure 2H. Note that this is the case even though the fits of the A-exciton to only one Lorentzian after Adjacent Average smoothing were not always of good quality (compare Figure 2F, 22–74 kg). Again, we obtain a refined equation to determine $\langle N \rangle_{\text{VF-weighted}}$ from the A-exciton energy, E_A , according to Eq. (4):

$$\langle N \rangle_{\text{VF-weighted}} = 10^{\frac{2.035 - E_A}{0.068}} \quad (4)$$

This underlines that not only is the size selection robust and reproducible, but also the data analysis and the established quantitative metrics for nanosheet length and thickness based on the extinction spectra.

In the following, we will focus on the previously proposed metrics to extract the ML V_f of liquid-exfoliated WS₂ from Raman/photoluminescence spectra.^[24] Since only monolayered WS₂ is a direct bandgap semiconductor showing appreciable photoluminescence (PL),^[38,39] the PL intensity should scale with the monolayer content. A suitable measure for the PL intensity can be obtained by subjecting the dispersions to Raman spectroscopy. If the excitation wavelength is chosen appropriately, both WS₂ Raman modes from all WS₂ units, as well as photoluminescence from the monolayer can be recorded simultaneously. Example spectra normalised to the main Raman mode (2LA(M) at 350 cm^{-1})^[40] of the two WS₂ batches excited with 532 nm are shown in Figure 3A,B. In addition to the Raman modes of WS₂ at ≈ 150 – 550 cm^{-1} , a group of features is observed at $>2000\text{ cm}^{-1}$. The PL from WS₂ is centered at $\approx 2500\text{ cm}^{-1}$ and predominantly stems from excitonic emission with negligible contribution from trions (see below and SI). The signals at $>3000\text{ cm}^{-1}$ (marked by *) are the Raman modes of water. As expected, the WS₂ PL increases with increasing monolayer content in the dispersions. Additional data where batch 2 is excited with 473 nm is shown in the SI (Figure S10).

A worry about using the intensity ratio of PL/Raman for a quantification of the ML V_f is that photoluminescence is extremely sensitive to the defect content in the samples as well as the dielectric environment.^[34,36,41–48] We therefore first test whether we can see a difference in the PL response in the two sample batches. It is important to note that batch 2 only contains 0.1 g L^{-1} SC surfactant, while batch 1 was redispersed in 2 g L^{-1} SC. In addition, two different batches of WS₂ starting material were used (albeit from the same distributor). To analyse the PL, the x-axis was converted into eV and the respective spectra fit to two Lorentzians for exciton and trion emission, as well as a component for the Raman mode of water where required. Fits are shown in the Supporting Information, Figures S11–S13. Similar to previous reports,^[42] Lorentzians describe the data very well. In all cases, the PL is dominated by emission from exciton with a minor species at lower energy which is attributed to emission from charged excitons (trions) which are often observed in TMDs.^[49–51]

Since the trion contribution is minor, we focus on an analysis of the exciton and extract energy as well as width from the fits. This data is plotted in Figure 3C,D as function of RCF. For batch 1, we see no shifts in the PL energy as function of RCF and hence

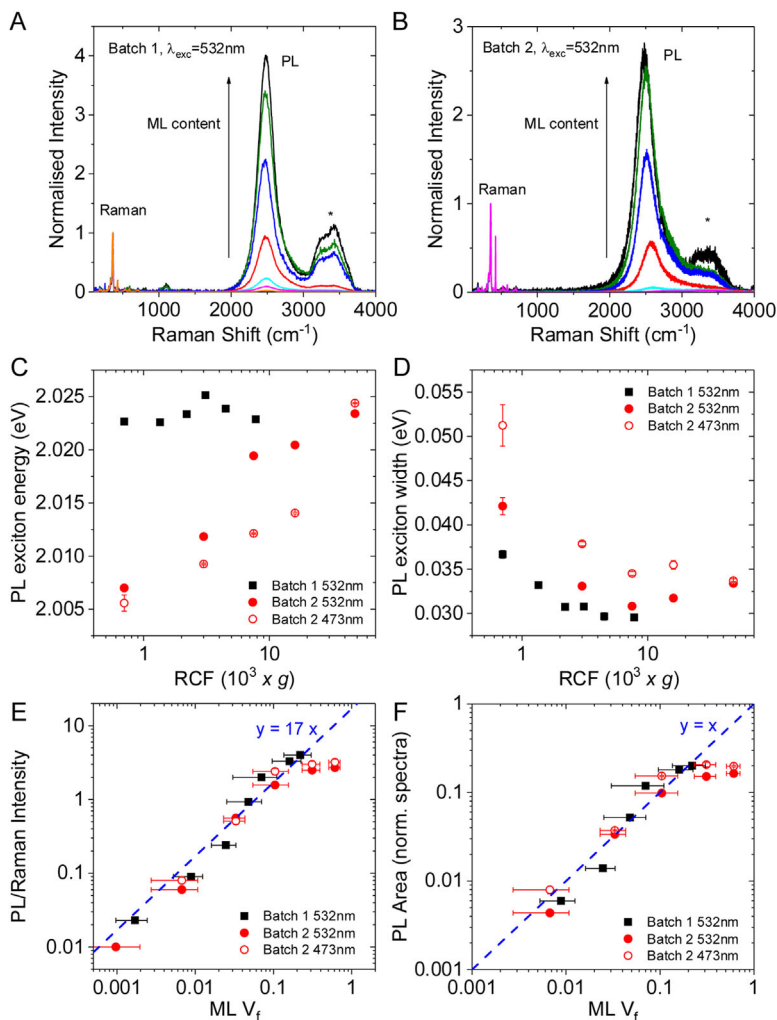


Figure 3. Raman/photoluminescence spectroscopy and derived monolayer content metrics for two batches of liquid-exfoliated WS₂. A–B) Raman spectra (532 nm excitation) of a range of size-selected WS₂ dispersions. Spectra are normalised to the WS₂ 2LA(M) Raman mode at 360 cm^{−1}. The photoluminescence predominantly from WS₂ monolayers is centred at 2500 cm^{−1}. The * indicates the Raman modes of water. A) Batch 1, B) Batch 2. C) Photoluminescence energy of the exciton (obtained from fitting) as function of the central centrifugal acceleration in the size selection cascade. For batch 2, data obtained from Raman/PL measurements using 473 nm excitation is included. D) Photoluminescence width of the exciton as function of RCF. E) PL/Raman intensity ratio as function of ML V_f. The blue dashed line is a linear fit which allows to extract ML V_f via Eq. (5). F) PL area obtained from fitting the PL in the spectra normalised to the most dominant Raman mode as function ML V_f. Fitting gives $\gamma = x$ (blue dashed line).

size with data centred around 2.024 eV (Figure 3C). In contrast, batch 2 shows a systematically decrease in the A-exciton PL with decreasing RCF (i.e. increasing nanosheet size) for both excitation wavelengths tested (532 and 473 nm). This is difficult to rationalise, as it is not observed for batch 1. In turn, the PL width decreases with increasing RCF in both cases, albeit with different absolute values for both batches (Figure 3D).

In general, three factors can have an impact on the PL peak position and width: i) temperature; ii) defect content; and iii) dielectric screening from different environments.^[34,36,41–48,51–53]

We can exclude temperature (potentially occurring due to measurement in different Raman setups) as a source for the deviation between the two batches with respect to exciton energy, as temperature would also strongly affect the exciton-trion ratio.^[51,53] This can also be observed in LPE TMDs when the laser power is varied (Figure S14). However, the exciton-trion ratio does not systematically change across these samples (Figure S15). The changes in PL width would suggest a variation in the defect content both across size-selected samples as well as slightly across the two batches. If we consider the width as an indicator for the defect content, laterally larger monolayers (enriched at low RCF) would have a higher defect content compared to smaller nanosheets. In addition, batch 2 could be slightly more defective compared to batch 1. Note that batch 2 was exfoliated using lower sonication power, so this is likely not due to defects introduced on exfoliation, but rather an effect of the starting material. However, even if the defect content between the two batches was different, this would not explain why they behave differently in their scaling of the exciton energy with RCF. We therefore suggest that the different scaling of the exciton energy with RCF is related to environmental effects. While batch 1 was measured in 2 g L^{−1} SC, only 0.1 g L^{−1} was used for batch 2. Especially the larger/thicker samples were kept at high nanosheet concentration (>2 g L^{−1}), while samples that are smaller/thinner had a lower nanosheet concentration (≈0.5 g L^{−1}) as can be clearly seen from the increasing Raman mode of water with increasing monolayer content (* in Figure 3B). It is thus plausible, that the SC concentration of 0.1 g L^{−1} was not sufficient to fully cover the nanosheets with surfactant. This results in a different effective dielectric environment which can lead to peak shifts across the size-selected samples as observed for batch 2.^[36,42–44]

While future research will be required to fully understand the PL of the LPE nanosheets, it is clear from the plots in Figure 3E,F that the previously suggested monolayer content metrics are surprisingly robust in spite of potential changes in defect content and solvatochromism across samples. In Figure 3E, we plot the PL/Raman intensity ratio as function of ML V_f, (determined from AFM) for both batches including two excitation wavelengths. All data, except the smallest nanosheets in batch 2 ($\langle L \rangle_{\text{cor}} < 20$ nm) fall on a mastercurve. The smallest nanosheets show a lower PL/Raman ratio as previously observed^[24] suggesting that PL is quenched in the edge region of the LPE nanosheets. Regardless of this, the previously established relation of the ML V_f to the PL/Raman intensity ratio via Eq. (5) is confirmed:

$$\text{ML } V_f [\%] = 5.9 \frac{I_{\text{PL}}}{I_{\text{Raman}}} \quad (5)$$

Alternatively, the fitted PL area in the spectra normalised to the Raman mode can be used as a measure of photoluminescence

intensity. In Figure 3F, it is shown that the PL area (sum of exciton and trion) scales directly as $\gamma = x$ with ML V_f . Even though fitting is required to obtain the area reliably, this quantification may be useful when a larger contribution from trion to the PL is present in the samples. Finally, we would like to emphasise that the scaling of the PL intensity with the ML V_f is equal for excitation with 532 and 473 nm. This is quite interesting because a different Raman mode was used for the normalisation of the spectra. An explanation for this phenomenon is beyond the scope of the manuscript.

3. Conclusions

In this manuscript we provided a spectroscopic and microscopic comparison of two batches of liquid-exfoliated WS₂ size-selected by cascade centrifugation. Different equipment was used in each step of sample preparation and characterisation. We showed that the size selection is very robust, as both L and N scale with the central g -force in the cascade even when different centrifugation setups are used. Note that this is only the case when filling heights and centrifugation times are similar. Furthermore, the refined microscopy statistics could be used to derive well defined quantitative relationships between arithmetic mean thickness, V_f -weighted thickness and monolayer content making it now possible to readily extract the monolayer content in the dispersions from the arithmetic mean thickness.

The previously established metrics for nanosheet size and thickness due to edge and confinement effects via extinction spectroscopy were shown to be robust with data from both batches collapsing on the same curve. A refined data analysis was elaborated for extinction spectra recorded with different settings. Due to the now available larger spread in $\langle N \rangle$ and $\langle L \rangle$, refined quantitative metric equations were presented.

Finally, the manuscript addressed the question whether the intensity of the PL relative to the Raman mode of the WS₂ provides a robust measure for the ML V_f . Importantly, this is indeed the case with the data from both batches collapsing on the same curve. In addition, excitation with a different wavelength resulted in the same quantitative relationship. We note that this is the case even though the PL is very sensitive to the environment and defect content in the samples. In the presented data, this lead to a variation in emission energy and PL width across the samples, but had no impact on the PL/Raman metric.

The demonstration of the robustness of size selection and metrics is an important part to utilise these techniques for further sample optimisation and potentially implementation in standardisation. In addition, part of the knowledge such as the well-defined scaling of nanosheet mean thickness and ML V_f can be directly applied to other layered materials size-selected by cascade centrifugation. The detailed analysis of the monolayer PL from LPE WS₂ suggests that the understanding of the PL and its scaling with dielectric environment and defects will be a key for defect engineering in TMDs due to the sensitivity of this readily available spectroscopy technique.

4. Experimental Section

Batch 1—Sample Preparation: See Ref. [24].

WS₂ dispersions were prepared by probe sonicating the powder (Sigma Aldrich, order number C1254-100G, initial concentration 20 g L⁻¹) in an aqueous sodium cholate (SC) solution. WS₂ was immersed in 80 mL of aqueous surfactant solution ($C_{SC} = 6 \text{ g L}^{-1}$). The mixture was sonicated under ice-cooling in a 100 mL metal beaker by probe sonication using a solid flathead tip (Sonics VXC-750, i.e., 750 W) for 1 h at 60% amplitude with a pulse of 6 s on and 2 s off. During the sonication, the sonic probe was placed 1.5 cm from the bottom of the beaker. The dispersion was centrifuged in 15 mL aliquots using 28 mL vials in a Hettich Mikro 220R centrifuge equipped with a fixed-angle rotor 1016 at 5 krpm (2660 g) for 1.5 h. The supernatant was discarded and the sediment collected in 80 mL of fresh surfactant ($C_{SC} = 2 \text{ g L}^{-1}$) and subjected to a second sonication using a solid flathead tip (Sonics VX-750) for 5 h at 60% amplitude with a pulse of 6 s on and 2 s off. From our experience, this two-step sonication procedure yields a higher concentration of exfoliated WS₂ and removes impurities.

To select nanosheets by size, we used liquid cascade centrifugation (Hettich Mikro 220R centrifuge, 15 °C) with sequentially increasing rotation speeds. Two different rotors were used. For speeds ≤ 5 krpm, a fixed angle rotor 1016 was used (28 mL vials, 10 mL aliquots in each vial). For this centrifuge and this rotor, the centrifugation rate, f , is related to the centrifugal force via $RCF = 106.4 f^2$ where f is the rotation rate in krpm. For speeds > 5 krpm, samples were centrifuged in a 1195-A fixed angle rotor (1.5 mL vials), where f is related to the centrifugal force via $RCF = 97.4 f^2$. The following procedure was applied as standard size selection of the primary cascade: Unexfoliated WS₂ was removed by centrifugation at 1.5 krpm (240 g, 2 h). The supernatant was subjected to further centrifugation at 2 krpm (426 g, 2 h). The sediment was collected in fresh surfactant ($C_{SC} = 2 \text{ g L}^{-1}$) at reduced volume (3–8 mL), while the supernatant was centrifuged at 3 krpm (958 g, 2 h). Again, the sediment was collected and the supernatant subjected to centrifugation at higher speeds. This procedure was repeated with the following speeds: 4 krpm (1700 g, 2 h), 5 krpm (2660 g, 2 h), 6 krpm (3506 g, 2 h), 7.5 krpm (5480 g, 2 h), 10 krpm (9740 g, 2 h). Throughout this manuscript, we use the central g -force to express the consecutive centrifugation. For example, the sediment collected from the centrifugation between 2 and 3 krpm has a central rpm of 2.5 krpm (665 g). Note that due to the different centrifuges used in this study, centrifugation conditions are expressed as relative centrifugal acceleration (RCF) in units of $10^3 \times g$ (or kg) with g being the gravitational force.

Batch 2—Sample preparation: Sample preparation was performed in analogy to batch 1, except for using different equipment and size selection conditions.

Exfoliation: Sonication Sonics VXC-500 tip sonicator (500 W), 60% amplitude, probe with replaceable end and a chiller system to maintain the temperature surrounding the sample beaker at 5 °C. The WS₂ powder was also purchased from Sigma Aldrich (order number C1254-100G), but a different batch was used.

Centrifugation: Beckman Coulter Avanti XP centrifuge with two different rotors. For centrifugation at $< 15\,000 \times g$, the JA25.50 fixed angle rotor and 50 mL centrifuge tubes (VWR, order number 525-0402) were used filled with 20 mL of dispersion each. For centrifugation at $> 15\,000 \times g$, the JA25.15 rotor was used with 14 mL vials (Beckman Coulter, order number 331374), filled with 10 mL dispersion each.

Compared to batch 1, different g -forces were used as boundaries in the cascade and sediments were collected in $c_{SC} = 0.1 \text{ g L}^{-1}$. RCF: 0.1 kg (discard sediment), 0.4 kg (collect 0.1–0.4 kg), 1 kg (collect 0.4–1 kg), 5 kg (collect 1–5 kg), 10 kg (collect 5–10 kg), 22 kg (collect 10–22 kg), 74 kg (collect 22–74 kg).

Batch 1—Characterisation: Atomic force microscopy (AFM) was carried out on a Veeco Nanoscope-IIIa (Digital Instruments) system equipped with a E-head (13 μm scanner) in tapping mode after depositing a drop of the dispersion (10 μL) on a pre-heated (150 °C) Si/SiO₂ wafer with an oxide layer of 300 nm. The high concentration dispersions collected after LCC were diluted with water (to optical densities at C-exciton of 0.1–0.2) immediately prior to deposition to reduce surfactant concentrations. After deposition, the wafer was rinsed with $\approx 5 \text{ mL}$ of water and $\approx 5 \text{ mL}$ of isopropanol. Typical image sizes ranged from $1 \times 1 \mu\text{m}^2$ to maximum

$4 \times 4 \mu\text{m}^2$ for the larger nanosheets at scan rates of 0.4–0.6 Hz with 512 lines per image. The apparent thickness was converted to number of layers using previously elaborated step-height analysis of liquid-exfoliated nanosheets.^[24,32]

Optical extinction was measured on a Varian Cary 500 in quartz cuvettes with a pathlength of 0.4 cm in 1 nm increments.

Raman/photoluminescence spectroscopy was performed on the liquid dispersions using a Horiba Jobin Yvon LabRAM HR800 with 532 nm excitation laser in air under ambient conditions. The Raman/PL emission was collected by $100\times$ long working distance objective and dispersed by 600 gr mm^{-1} with 10% of the laser power ($\approx 2 \text{ mW}$). Great care must be taken during these measurements, as changes in the focal plane during the acquisition will introduce an error in the PL/Raman ratio. This is often reflected in a tilted baseline or asymmetric PL due to innerfilter and reabsorption effects. It can also be visually recognized when the size of the laser spot in the optical image has changed during the measurement. The average of ≈ 5 measurements are displayed. Acquisition times were kept as short as possible depending on the concentration of the dispersion (between 2 and 10 s per frame, 4 frames were covered in each measurement).

Batch 2–Characterisation: Characterisation was performed in analogy to batch 1, except for using different equipment.

AFM: Dimension ICON3 scanning probe microscope (Bruker AXS S.A.S.) with a $60 \mu\text{m}^2$ scan head in tapping mode in air under ambient conditions using aluminium coated silicon cantilevers (OTESP-R3). Image sizes for small nanosheets were $5 \times 5 \mu\text{m}^2$ with 1024 lines, and $10 \times 10 \mu\text{m}^2$ with 1024 lines per image in the case of larger nanosheets, respectively.

Optical extinction: Varian Cary 5000i in quartz cuvettes with a pathlength of 0.4 cm in 0.5 nm increments.

Raman 532 nm: Renishaw InVia microscope. The Raman emission was collected by a $50\times$, long working distance objective lens in streamline mode and dispersed by a 2400 l/mm grating with 5% of the laser power ($< 1 \text{ mW}$). Acquisition times were 10 s per spectrum.

Raman 473 nm: Horiba LabRAM Evolution microscope. The Raman emission was collected by a $50\times$, long working distance objective lens and dispersed by a 1800 l/mm grating with 10% of the laser power ($< 0.75 \text{ mW}$). Acquisition times were 10 s per spectrum.

Supporting Information

The Supporting Information is available from the Wiley Online Library or from the author.

Acknowledgements

C.B. acknowledges the German research foundation DFG under Emmy-Noether grant BA4856/2-1. We thank Jana Zaumseil for the access to the full infrastructure of the Chair of Applied Physical Chemistry in Heidelberg.

Conflict of Interest

The authors declare no conflict of interest.

Keywords

centrifugation, layered materials, liquid exfoliation, optical properties, transition metal dichalcogenides, WS_2

Received: August 16, 2017

Revised: October 3, 2017

Published online:

- [1] D. Jariwala, V. K. Sangwan, L. J. Lauhon, T. J. Marks, M. C. Hersam, *ACS Nano* **2014**, *8*, 1102.
- [2] K. F. Mak, J. Shan, *Nat. Photon* **2016**, *10*, 216.
- [3] M. Buscema, J. O. Island, D. J. Groenendijk, S. I. Blanter, G. A. Steele, H. S. J. van der Zant, A. Castellanos-Gomez, *Chem. Soc. Rev.* **2015**, *44*, 3691.
- [4] D. Voiry, J. Yang, M. Chhowalla, *Adv. Mater.* **2016**, *28*, 6197.
- [5] T. Low, A. Chaves, J. D. Caldwell, A. Kumar, N. X. Fang, P. Avouris, T. F. Heinz, F. Guinea, L. Martin-Moreno, F. Koppens, *Nat. Mater.* **2017**, *16*, 182.
- [6] B. L. Li, J. Wang, H. L. Zou, S. Garaj, C. T. Lim, J. Xie, N. B. Li, D. T. Leong, *Adv. Funct. Mater.* **2016**, *26*, 7034.
- [7] H. Tao, Y. Gao, N. Talreja, F. Guo, J. Texter, Z. Sun, C. Yan, *J. Mater. Chem. C* **2017**, *16*.
- [8] M. Pumera, Z. Sofer, A. Ambrosi, *J. Mater. Chem. C* **2014**, *2*, 8981.
- [9] B. Mendoza-Sánchez, Y. Gogotsi, *Adv. Mater.* **2016**, *28*, 6104.
- [10] A. G. Kelly, T. Hallam, C. Backes, A. Harvey, A. S. Esmaeily, I. Godwin, J. Coelho, V. Nicolosi, J. Lauth, A. Kulkarni, S. King, L. D. A. Siebbeles, G. S. Duesberg, J. N. Coleman, *Science* **2017**, *356*, 69.
- [11] D. McManus, S. Vranic, F. Withers, V. Sanchez-Romaguera, M. Macucci, H. Yang, R. Sorrentino, K. Parvez, S.-K. Son, G. Iannaccone, K. Kostarelos, G. Fiori, C. Casiraghi, *Nat. Nanotechnol.* **2017**, *12*, 343.
- [12] X. Cao, C. Tan, X. Zhang, W. Zhao, H. Zhang, *Adv. Mater.* **2016**, *28*, 6167.
- [13] F. Bonaccorso, A. Bartolotta, J. N. Coleman, C. Backes, *Adv. Mater.* **2016**, *28*, 6136.
- [14] V. Nicolosi, M. Chhowalla, M. G. Kanatzidis, M. S. Strano, J. N. Coleman, *Science* **2013**, *340*, 1420.
- [15] A. Ciesielski, P. Samori, *Chem. Soc. Rev.* **2014**, *43*, 381.
- [16] K. Parvez, S. Yang, X. Feng, K. Müllen, *Synth. Met.* **2015**, *210*, 123.
- [17] M. Yi, Z. Shen, *J. Mater. Chem. C* **2015**, *3*, 11700.
- [18] E. D. Grayfer, M. N. Kozlova, V. E. Fedorov, *Adv. Colloid Interface Sci.* **2017**, *245*, 40.
- [19] H. Tao, Y. Zhang, Y. Gao, Z. Sun, C. Yan, J. Texter, *Phys. Chem. Chem. Phys.* **2017**, *19*, 921.
- [20] J. N. Coleman, M. Lotya, A. O'Neill, S. D. Bergin, P. J. King, U. Khan, K. Young, A. Gaucher, S. De, R. J. Smith, I. V. Shvets, S. K. Arora, G. Stanton, H.-Y. Kim, K. Lee, G. T. Kim, G. S. Duesberg, T. Hallam, J. J. Boland, J. J. Wang, J. F. Donegan, J. C. Grunlan, G. Moriarty, A. Shmeliov, R. J. Nicholls, J. M. Perkins, E. M. Grieveson, K. Theuvsen, D. W. McComb, P. D. Nellist, V. Nicolosi, *Science* **2011**, *331*, 568.
- [21] R. J. Smith, P. J. King, M. Lotya, C. Wirtz, U. Khan, S. De, A. O'Neill, G. S. Duesberg, J. C. Grunlan, G. Moriarty, J. Chen, J. Wang, A. I. Minett, V. Nicolosi, J. N. Coleman, *Adv. Mater.* **2011**, *23*, 3944.
- [22] J. Kang, V. K. Sangwan, J. D. Wood, M. C. Hersam, *Acc. Chem. Res.* **2017**, *50*, 943.
- [23] F. Bonaccorso, A. Lombardo, T. Hasan, Z. Sun, L. Colombo, A. C. Ferrari, *Mater. Today* **2012**, *15*, 564.
- [24] C. Backes, B. M. Szydlowska, A. Harvey, S. Yuan, V. Vega-Mayoral, B. R. Davies, P.-I. Zhao, D. Hanlon, E. J. G. Santos, M. I. Katsnelson, W. J. Blau, C. Gadermaier, J. N. Coleman, *ACS Nano* **2016**, *10*, 1589.
- [25] D. Hanlon, C. Backes, E. Doherty, C. S. Cucinotta, N. C. Berner, C. Boland, K. Lee, P. Lynch, Z. Gholamvand, A. Harvey, S. Zhang, K. Wang, G. Moynihan, A. Pokle, Q. M. Ramasse, N. McEvoy, W. J. Blau, J. Wang, G. Abellan, F. Hauke, A. Hirsch, S. Sanvito, D. D. O'Regan, G. S. Duesberg, V. Nicolosi, J. N. Coleman, *Nature Commun.* **2015**, *6*, 8563.
- [26] A. Harvey, C. Backes, Z. Gholamvand, D. Hanlon, D. McAteer, H. C. Nerl, E. McGuire, A. Seral-Ascaso, Q. M. Ramasse, N. McEvoy, S. Winters, N. C. Berner, D. McCloskey, J. Donegan, G. Duesberg, V. Nicolosi, J. N. Coleman, *Chem. Mater.* **2015**, *27*, 3483.

- [27] C. Backes, K. R. Paton, D. Hanlon, S. Yuan, M. I. Katsnelson, J. Houston, R. J. Smith, D. McCloskey, J. F. Donegan, J. N. Coleman, *Nanoscale* **2016**, *8*, 4311.
- [28] Z. Gholamvand, D. McAteer, A. Harvey, C. Backes, J. N. Coleman, *Chem. Mater.* **2016**, *28*, 2641.
- [29] A. Harvey, X. He, I. J. Godwin, C. Backes, D. McAteer, N. C. Berner, N. McEvoy, A. Ferguson, A. Shmeliov, M. E. G. Lyons, V. Nicolosi, G. S. Duesberg, J. F. Donegan, J. N. Coleman, *J. Mater. Chem. C* **2016**, *4*, 11046.
- [30] H. Sun, A. Varzi, V. Pellegrini, D. A. Dinh, R. Raccichini, A. E. Del Rio-Castillo, M. Prato, M. Colombo, R. Cingolani, B. Scrosati, S. Passerini, F. Bonaccorso, *Solid State Commun.* **2017**, *251*, 88.
- [31] S. Mandeep, G. Enrico Della, A. Taimur, W. Sumeet, R. Rajesh, E. Joel van, M. Edwin, B. Vipul, *2D Mater.* **2017**, *4*, 025110.
- [32] C. Backes, R. J. Smith, N. McEvoy, N. C. Berner, D. McCloskey, H. C. Nerl, A. O'Neill, P. J. King, T. Higgins, D. Hanlon, N. Scheuschner, J. Maultzsch, L. Houben, G. S. Duesberg, J. F. Donegan, V. Nicolosi, J. N. Coleman, *Nat. Commun.* **2014**, *5*, 4576.
- [33] A. Harvey, C. Backes, Z. Gholamvand, D. Hanlon, D. McAteer, H. C. Nerl, E. McGuire, A. Seral-Ascaso, Q. M. Ramasse, N. McEvoy, S. Winters, N. C. Berner, D. McCloskey, J. F. Donegan, G. S. Duesberg, V. Nicolosi, J. N. Coleman, *Chem. Mater.* **2015**, *27*, 3483.
- [34] K. F. Mak, C. Lee, J. Hone, J. Shan, T. F. Heinz, *Phys. Rev. Lett.* **2010**, *105*, 136805/136801.
- [35] A. Splendiani, L. Sun, Y. Zhang, T. Li, J. Kim, C.-Y. Chim, G. Galli, F. Wang, *Nano Lett.* **2010**, *10*, 1271.
- [36] A. Raja, A. Chaves, J. Yu, G. Arefe, H. M. Hill, A. F. Rigosi, T. C. Berkelbach, P. Nagler, C. Schüller, T. Korn, C. Nuckolls, J. Hone, L. E. Brus, T. F. Heinz, D. R. Reichman, A. Chernikov, *Nat. Commun.* **2017**, *8*, 15251.
- [37] L. Yadgarov, C. L. Choi, A. Sedova, A. Cohen, R. Rosentsveig, O. Bar-Elli, D. Oron, H. Dai, R. Tenne, *ACS Nano* **2014**, *8*, 3575.
- [38] H. R. Gutiérrez, N. Perea-López, A. L. Elías, A. Berkdemir, B. Wang, R. Lv, F. López-Urías, V. H. Crespi, H. Terrones, M. Terrones, *Nano Lett.* **2012**, *13*, 3447.
- [39] W. Zhao, Z. Ghorannevis, L. Chu, M. Toh, C. Kloc, P.-H. Tan, G. Eda, *ACS Nano* **2012**, *7*, 791.
- [40] X. Zhang, X.-F. Qiao, W. Shi, J.-B. Wu, D.-S. Jiang, P.-H. Tan, *Chem. Soc. Rev.* **2015**, *44*, 2757.
- [41] N. Mao, Y. Chen, D. Liu, J. Zhang, L. Xie, *Small* **2013**, *9*, 1312.
- [42] Y. Lin, X. Ling, L. Yu, S. Huang, A. L. Hsu, Y.-H. Lee, J. Kong, M. S. Dresselhaus, T. Palacios, *Nano Lett.* **2014**, *14*, 5569.
- [43] S. Mouri, Y. Miyauchi, K. Matsuda, *Nano Lett.* **2013**, *13*, 5944.
- [44] N. Peimyoo, W. Yang, J. Shang, X. Shen, Y. Wang, T. Yu, *ACS Nano* **2014**, *8*, 11320.
- [45] M. Amani, D.-H. Lien, D. Kiriya, J. Xiao, A. Azcatl, J. Noh, S. R. Madhupathy, R. Addou, S. KC, M. Dubey, K. Cho, R. M. Wallace, S.-C. Lee, J.-H. He, J. W. Ager, X. Zhang, E. Yablonovitch, A. Javey, *Science* **2015**, *350*, 1065.
- [46] L. Yuan, L. Huang, *Nanoscale* **2015**, *7*, 7402.
- [47] H. Wang, C. Zhang, F. Rana, *Nano Lett.* **2015**, *15*, 339.
- [48] L. Zhong, R. C. Bruno, K. Ethan, L. Ruitao, R. Rahul, T. Humberto, A. P. Marcos, T. Mauricio, *2D Mater.* **2016**, *3*, 022002.
- [49] K. F. Mak, K. He, C. Lee, G. H. Lee, J. Hone, T. F. Heinz, J. Shan, *Nature Mater.* **2013**, *12*, 207.
- [50] J. S. Ross, S. Wu, H. Yu, N. J. Ghimire, A. M. Jones, G. Aivazian, J. Yan, D. G. Mandrus, D. Xiao, W. Yao, X. Xu, *Nat. Commun.* **2013**, *4*, 1474.
- [51] A. A. Mitoglu, P. Plochocka, J. N. Jadcak, W. Escoffier, G. L. J. A. Rikken, L. Kulyuk, D. K. Maude, *Phys. Rev. B* **2013**, *88*, 245403.
- [52] Z. He, X. Wang, W. Xu, Y. Zhou, Y. Sheng, Y. Rong, J. M. Smith, J. H. Warner, *ACS Nano* **2016**, *10*, 5847.
- [53] K. M. McCreary, A. T. Hanbicki, S. Singh, R. K. Kawakami, G. G. Jernigan, M. Ishigami, A. Ng, T. H. Brintlinger, R. M. Stroud, B. T. Jonker, *Sci. Rep.* **2016**, *6*, 35154.
- [54] C. Backes, T. M. Higgins, A. Kelly, C. Boland, A. Harvey, D. Hanlon, J. N. Coleman, *Chem. Mater.* **2017**, *29*, 243.